Understanding the origins of N2O decomposition activity in Mn(Fe)CoAlO hydrotalcite derived mixed metal oxides

Magdalena Jabłońska, Miren Agote Arán, Andrew M. Beale, Gerard Delahay, Carolina Petitto, Marek Nocuń, Regina Palkovits

Understanding the origins of N_2O decomposition activity in Mn-Co-Al-O_x hydrotalcite derived mixed metal oxides.

Magdalena Jabłońska[a,b]*, Miren Agote Arán[c,d], Andrew M. Beale[c,d], Gérard Delahay[e], Carolina Petitto[e], Marek Nocuń[f], Regina Palkovits[a,b]*

[a]*Institut für Technische und Makromolekulare Chemie, Chair of Heterogeneous Catalysis and Chemical Technology, RWTH Aachen University, Worringerweg 2, 52074 Aachen, Germany*

[b]*Center for Automotive Catalytic Systems Aachen – ACA, RWTH Aachen University, Schinkelstr. 8, 52062 Aachen, Germany*

[c]*UK Catalysis Hub, Research Complex at Harwell, Rutherford Appleton Laboratories, Didcot, Oxon OX11 0FA, U.K.*

[d]*Department of Chemistry, University College London, 20 Gordon Street, London, WC1H 0AJ, U.K.*

[e]*Institut Charles Gerhardt de Montpellier, 240 avenue du Professeur Emile Jeanbrau, 34296 Montpellier Cedex 5, France*

[f]*Faculty of Material Science and Ceramics, AGH University of Science and Technology, Mickiewicza 30, 30-059 Kraków, Poland*

*Corresponding author. Tel: +49 241 80 26497; Fax: +49 241 80 22177. *E-mail address*: Palkovits@itmc.rwth-aachen.de (R. Palkovits), Jablonska@itmc.rwth-aachen (M. Jabłońska)

Abstract

The catalytic decomposition of N_2O was studied over a series of calcined (Mn,Fe)-Co-Al hydrotalcite-like compounds. The precursors were prepared by coprecipitation and characterized by XRD and TGA. While the mixed metal oxides derived after calcination at 600 °C were characterized by XRD, N_2 adsorption, H_2-TPR and XPS. Moreover, *in situ* XAFS measurements over selected mixed metal oxides were performed. Such investigations under reaction conditions are rare, while a comprehensive understanding of the involved active

species may facilitate a knowledge-based catalyst optimization. The activity of the Co-Al (Co/Al = 3/1, mol.%) catalyst varied depending on the loading of Mn or Fe (0.0575, 0.0821, 0.1150, 0.1725, 0.2300, mol.%). In the investigated series, $Mn_{0.1725}Co_3A_l$ mixed metal oxides reached the highest activity with T_{50} of about 305 and 376 °C under N_2O/N_2 and $N_2O,NO,O_2/N_2$ feed, respectively. *In situ* X-ray absorption experiments over $Mn_{0.1725}Co_3A_lO_x$ suggested that $Mn_xCo_yO_4$ spinel undergo reduction to CoO and MnO upon heating up to 600 °C in He. Under N_2O/He conditions initial reoxidation of cobalt species began at 350 °C. The lower activity obtained for $Fe_{0.1725}Co_3A_lO_x$ is explained by the fact that the majority of Fe was not incorporated into the Co_3O_4 structure but instead formed less reactive iron oxide clusters.

Keywords: hydrotalcite-like compounds, mixed metal oxides, cobalt, N_2O decomposition, XAFS.

1. Introduction

The catalytic decomposition of N_2O (deN_2O) belongs to the best available technologies for N_2O abatement from nitric acid production, which is one of the major industrial sources of N_2O emission. The broad collection of catalysts were applied at temperatures below 450-500 °C [1]. As implied by the published results, hydrotalcite derived mixed metal oxides present high activity for deN_2O even in the presence of H_2O, O_2, SO_2 and/or NO_x. The hydrotalcite-like compounds with a general formula of $M^{2+}_{1-x}M^{3+}_x(OH)_2\,(A^{n-})_{x/n} \cdot mH_2O$, where M^{2+} and M^{3+} – bi- and trivalent metal cations, respectively, A^{n-} – an interlayer anion, and x – $M^{3+}/(M^{3+}+M^{2+})$ with a value between 0.17 - 0.50 [2,3], serve as excellent precursors for the preparation of the catalysts of the desired chemical and phase composition for deN_2O. Thermal decomposition of hydrotalcite-like compounds at middle temperatures (≤600 °C) results in the formation of the relatively high surface mixed metal oxides, with a high dispersion of introduced transition oxide metal species [4–6]. Recently, Jabłońska and Palkovits [1,7] reviewed hydrotalcite derived mixed metal oxides in deN_2O, and concluded that the activity of the mixed metal oxides varied depending on the type and loading of the catalytically active metal, its oxidation state as well as dispersion and aggregation state, etc. The research of hydrotalcite derived mixed metal oxides focusses mainly on cobalt-based materials: Co-Al-O_x (e.g. [8,9]), Co-(Mg)-Mn-(Al)-O_x (e.g. [10–12]), Co-Mg-

Al-O_x or Co-Cu-Mg-Al-O_x (e.g. [13]), etc. Kannan et al. [14–16] and furthermore Pérez-Ramírez et al. [8] found Co/Al with 3/1 molar ratio as optimal hydrotalcite derived catalyst dedicated to deN_2O among catalysts varied between Co/Al = 3-1/1, mol.%. The Co_3Al_1 mixed metal oxides reached 84-100% conversion at 450 °C. Kannan et al. [15,16] reported that the activity of Co-Al mixed metal oxides correlated with the Co/Al bulk composition, but, an even better correlation in the activity was obtained with the Co^{2+} (generated by surface reduction and reconstruction) of mixed metal oxides, as determined by XPS. Obalová et al. [10,11,17] investigated numerous combinations of Co(Mg)-Mn(Al), and found $Co_4Mn_1Al_1O_x$ as optimum catalyst for deN_2O (82-97% conversion at 450 °C). The authors reported an optimum surface amount of Co^{2+}/Co^{3+} and Mn^{2+}/Mn^{3+} molar ratios at 1.13 and 2.27 by XPS. Moreover, as determined from H_2-TPR, $Co_4Mn_1Al_1O_x$ possessed an optimum amount of components reducible in the temperatures of the maximum conversion of N_2O (between 350-450 °C) [11]. Since the detailed study of the involved active species of the hydrotalcite derived catalysts under reaction conditions was beyond of the previously published results~~. Thus, the above studies were the inspiration for~~ Our present investigation focused on identifying *in situ* the exact nature of cobalt species in Mn(Fe)CoAl ~~hydrotalcite-derived~~ mixed metal oxides applied to deN_2O. Moreover, precursors and/or mixed metal oxides were characterized by XRD, TG, N_2 adsorption and H_2-TPR, in order to explore additional structure-activity correlations.

2. Experimental

2.1. Catalysts preparation

A series of $Mn(Fe)_xCo_3Al_1$ (x = 0.0575, 0.0821, 0.1150, 0.1725, 0.2300, mol.%) hydrotalcite-like compounds was prepared by the coprecipitation. An aqueous solution containing appropriate amounts of following metal nitrates: $Co(NO_3)_2 \cdot 6H_2O$ (Roth), $Al(NO_3)_3 \cdot 9H_2O$ (Sigma), $Mn(NO_3)_2 \cdot 4H_2O$ (Roth), $Fe(NO_3)_3 \cdot 9\ H_2O$ (Roth) and 1 M NaOH (Chemsolute) was dropped simultaneously to a vigorously stirred at 60 °C aqueous solution containing a slight over-stoichiometric excess of Na_2CO_3 (Sigma). The pH of the reaction mixture was maintained constant at 10.0 ± 0.2 throughout the whole synthesis by NaOH addition. The obtained suspension was aged at 60 °C for another 0.5 h after complete coprecipitation. The solid was filtered, washed carefully

with distilled water and dried at room temperature. Finally, the prepared hydrotalcite-like compounds were crushed and calcined at 600 °C for 6 h with a heating ramp of 10 °C/min and in static air. The hydrotalcite derived mixed metal oxides were kept in a desiccator in order to avoid the reconstruction of the hydroxide-like structure. For catalytic experiments, a fraction of particle size in the range of 0.250-0.500 mm was used.

2.2. Catalysts characterization

The X-Ray diffraction (XRD) measurements of the all as-synthesized hydrotalcite-like compounds and mixed metal oxides formed by their thermal decomposition was performed applying a Siemens D5000 XRD diffractometer using Cu-Kα radiation (λ = 1.54056 Å, 45 kV, 40 mA). The difference thermogravimetric analysis (DTG) of the hydrotalcite-like compounds (~20 mg) was carried out using a Netzsch STA 409C/CD operated under a flow of air (10 cm^3/min) in the temperature range of 30-1000 °C with a linear heating rate of 5 °C /min. The specific surface area (S_{BET}) of the mixed metal oxides was determined by low-temperature (-196 °C) N_2 sorption using a Quantachrome Quadrasorb SI. Prior to nitrogen adsorption the samples were outgassed at 250 °C for 12 h using a Quantachrome Flovac degasser. The specific surface area (S_{BET}) was calculated using the Brunauer-Emmett-Teller (BET) multiple point method in the p/p_0 range from 0.05 to 0.3. The chemical analysis of mixed metal oxides was determined by ICP-MS using an Agilent Technologies 8800 Triple Quad spectrometer. Prior to measurement, sample (50 mg) was dissolved in 6 cm^3 mixture of concentrated acids (HCl:HNO_3, 1:1), and afterwards the resulted mixture was diluted with 64 cm^3 deionized water before warming up to 40 °C for 24 h. The redox properties of the selected mixed metal oxides were studied by the temperature-programmed reduction (H_2-TPR) using Quantachrome ChemBET Pulsar TPR/TPD. H_2-TPR runs for the samples (30 mg) were carried out starting from room temperature to 1000 °C, with a linear heating rate of 10 °C /min and in a flow (25 cm^3/min) of 5.0 vol.% H_2/Ar. Water vapour was removed from effluent gas by the means of a cold trap placed in an ice-water bath. The H_2 consumption was detected and recorded by TCD detector. The X-ray photoelectron spectra (XPS) of selected mixed metal oxides were measured on a VSW spectrometer equipped with a hemispherical analyzer. The photoelectron spectra were measured using a magnesium MgKα source (E = 1253.6 eV). The base pressure in the analysis chamber during the measurements was $3 \cdot 10^{-6}$ Pa and the spectra were calibrated on a main carbon C 1s peak at 284.6 eV. The composition and

chemical surrounding of the sample surface were investigated based on the areas and binding energies of Co 2p, Mn 2p, Fe 2p, Al 2p, O 1s and C 1s photoelectron peaks. Mathematical analyses of the XPS spectra were carried out using the XPSpeak 4.1 computer software (RWM. Kwok, The Chinese University of Hong Kong).

The X-ray absorption spectra (XAS) of selected samples were collected *in situ* using the quartz capillary flow reactor cells, and gas delivery systems available on the beamline, on station B18 at the Diamond Light Source synchrotron facility. The measurements were carried out using a Si(111) monochromator at the Co K-edge, Mn K-edge or Fe K-edge with the respective Co, Mn or Fe monometallic foils (10 μm) used as an energy calibrant for the monochromator. The catalyst diluted with SiO_2 (1:5) was sieved into 0.200-0.250 mm and placed into the reactor. Prior to the reaction the catalyst was outgassed at 600 °C for 1 h in a flow of pure He (10 cm^3/min), and subsequently cooled down to 100 °C. The reactant concentrations at the reactor inlet composed of [N_2O] = 0.1 vol.% and [He] = 99.9 vol.% (10 cm^3/min). The temperature was raised in steps of 50-100 °C up to 600 °C. Each temperature was hold for 30 min. X-ray absorption spectra at appropriate K-edges was collected in fluorescence mode for 240 s for Co, Fe or Mn K-edges. At least three spectra for each sample were taken at room temperature, appropriate temperatures and after reaction at room temperature. CoO, Co_3O_4, FeO, Fe_2O_3, MnO_2 references were measured only at room temperature. The data were analysed using the Demeter software package [18,19]); the edge position was determined as the first maximum – after the pre-edge peak – of the derivative of the XANES spectra.

2.3. Catalytic tests

The catalytic performance of the mixed metal oxides was evaluated in the N_2O decomposition. The catalytic experiments were carried out under atmospheric pressure in a fixed-bed flow microreactor (i.d., 6 mm; l., 270 mm). Prior to the reaction the catalyst (350 mg) was outgassed at 600 °C for 1 h in a flow of pure N_2 (100 cm^3/min). The reactant concentrations at the reactor inlet composed of: (i) [N_2O] = 0.1 vol.%, N_2 balance, (ii) [N_2O] = 0.1 vol.%, [NO] = 0.03 vol.%, [O_2] = 4.5 vol.%, N_2 balance (100 cm^3/min; WHSV = 17 L $(h\ g)^{-1}$, were analyzed by infrared spectroscopy using a Perkin Elmer Spectrum Two equipped with a Pike 5 m heated gas cell. The temperature was raised in steps of 50 °C starting from 100 up to 600 °C. Each temperature was set constant for 0.5 h.

For selected material, additional tests were carried out in the presence of water vapour. Such catalytic experiments were carried out under atmospheric pressure in a fixed-bed flow microreactor (i.d., X mm; l., X mm). Prior to the reaction, the catalyst (70-150 mg) was activated at 580 °C for 0.5 h in a flow of pure He (75 cm^3/min). After reactor cooled down, the following composition was applied: [N_2O] = 0.1 vol.%, ([H_2O] = 3.5 wt.%), He balance (75 cm^3/min; WHSV = 30-64 L $(h\ g)^{-1}$), were analyzed by a Pfeiffer Omnistar quadrupole mass spectrometer equipped with Channeltron and Faraday detectors (0-200 amu).

The conversion of N_2O ($X(N_2O)$) was estimated according to $X(N_2O) = ([c(N_2O)_{in}\text{-}c(N_2O)_{out}]/c(N_2O)_{in}) \times 100\%$, where: $c(N_2O)_{in}$ and $c(N_2O)_{out}$ – concentration of N_2O in the inlet gas, and concentration of N_2O in the outlet gas.

3. Results and discussion

Fig. 1 presents the XRD patterns of $Mn(Fe)_xCo_3Al_1$ (x = 0.0575, 0.0821, 0.1150, 0.1725, 0.2300, mol.%) hydrotalcite-like compounds, exhibiting rhombohedral symmetry (space group R3m, $3R_1$ polytype) [20] with sharp and symmetrical reflections (0 0 3), (0 0 6), (1 1 0) and (1 1 3), and broad and asymmetrical reflections (0 1 2), (0 1 5) and (0 1 8). The intensity of the reflection corresponding to the hydrotalcite-like phase were very weak for samples with 0.0575 mol.% of Mn or Fe. However, the intensity of such phases increased with increasing loading of both transition metals. Table 1 summarizes the unit cell parameters of the hydrotalcite-like compounds and their derivatives. The cell parameters were calculated using a position of (1 0 1) reflection: $a = 2(d_{1\,1\,0})$ and positions of basal reflections: $c = [3(d_{0\,0\,3}) + 6(d_{0\,0\,6})]/2$. The lattice paramater *a* depends on the size of the cation in the brucite-like layers, while the parameter *c* refers to the interlayer thickness. The *a* values for $Mn(Fe)_xCo_3Al_1$ (x = 0.0575, 0.0821, 0.1150, 0.1725, 0.2300, mol.%) hydrotalcite-like compounds varied only slightly with increasing Mn or Fe content and were close to the one obtained for Co_3Al_1. The *a* values depends mainly on the ionic radii of the cations in octahedral coordination (0.070 nm Co^{2+}, 0.070 nm Mn^{2+} and 0.070 nm Fe^{3+} [21], as cations of metal precursors). The *c* values of about 2.3 nm stay characteristic for hydrotalcite-like compounds containing carbonates located in the interlayer space [2]. The interlayer distances increased upon decreasing electronegativity of the cations: Co (1.70) > Fe (1.64) > Mn (1.60) > Al (1.47)

(according to Allred-Rochow scale) [22]. The crystal sizes were calculated from the Scherrer equation $D = 0.89 \cdot \lambda / \beta \cdot \theta$, where D is the crystallite size, λ is the X-ray wavelength, β is the line broadening and θ is the Bragg angle. The Fe-containing materials revealed overall higher crystal size (with the exception of $Fe_{0.0575}Co_3Al_1$) than corresponding $MnCo_3Al_1$ compounds.

Fig. 2 presents the DTG profiles of $Mn(Fe)_xCo_3Al_1$ (x = 0.0575, 0.0821, 0.1150, 0.1725, 0.2300, mol.%) hydrotalcite-like compounds, while Table 2 gathers total mass loss of these materials. DTG profiles revealed the presence of two stages of weight loss, providing an additional proof of the achievement of the hydrotalcite-like structure. The thermal decomposition of Mn(Fe)-Co-Al precursors proceeded in two main stages with total mass losses of about 30-33%. The first DTG minimum centered at about 190-200 °C corresponded to the removal of interlayer and weakly adsorbed water without collapse of the structure. The second peak located at about 230-235 °C appeared due to the dehydroxylation of the brucite-like layers and thermal decomposition of interlayer carbonates and nitrates (e.g. [5,6,20]). The temperatures and peak intensities did not change significantly among studied precursors, possibly due to small differences in the Mn or Fe loading as well as similar size of Mn^{2+} and Fe^{3+} (as cations of metal precursors) in octahedral coordination of ~~0.058 and 0.055~~ 0.070 nm~~, respectively~~ [21].

Fig. 3 shows the XRD patterns of calcined Mn(Fe)CoAl hydrotalcite-like compounds. The hydrotalcite-like structure was completely destroyed upon heating at 600 °C with possible formation of $Co_3O_4/CoAl_2O_4/Co_2AlO_4$ spinels (2θ at 19, 31, 37, 39, 45, 56, 59, 65, 77°) (e.g. [8,16]), exhibiting cubic symmetry (space group Fd3m) [24]. The lattice parameter *a* in the range of 0.8073-0.8099 nm was close to Co_3O_4 (*a* = 0.8084 nm). Mn- or Fe- containing materials did not reveal any diffraction characteristic for transition metal oxides in the XRD patterns, which confirmed the absence of bigger crystallites. Crystal sizes of 26-33 nm were calculated from (3 1 1) brag reflection in the XRD patterns using the Scherrer equation.

Fig. 1, Fig. 2, Fig. 3

Table 1. Lattice parameters of (Mn,Fe)-Co-Al hydrotalcite-like compounds and corresponding mixed metal oxides.

Hydrotalcite-like compounds	Cell parameter *a* [nm]	Cell parameter *c* [nm]	Crystallite size D*a* [nm]	Crystallite size D*c* [nm]	Mixed metal oxides	Cell parameter *a* [nm]	Crystallite size D*a* [nm]
Co_3Al_1	0.3079	2.2956	29	20	$Co_3Al_1O_x$	27	0.8093
$Mn_{0.0575}Co_3Al_1$	0.3085	2.3065	33	22	$Mn_{0.0575}Co_3Al_1O_x$	32	0.8076
$Mn_{0.0821}Co_3Al_1$	0.3086	2.3060	34	21	$Mn_{0.0821}Co_3Al_1O_x$	32	0.8083
$Mn_{0.1150}Co_3Al_1$	0.3085	2.3006	25	24	$Mn_{0.1150}Co_3Al_1O_x$	27	0.8099
$Mn_{0.1725}Co_3Al_1$	0.3080	2.2800	33	24	$Mn_{0.1725}Co_3Al_1O_x$	26	0.8079
$Mn_{0.2300}Co_3Al_1$	0.3078	0.2790	27	24	$Mn_{0.2300}Co_3Al_1O_x$	26	0.8099
$Fe_{0.0575}Co_3Al_1$	0.3085	2.3215	22	22	$Fe_{0.0575}Co_3Al_1O_x$	30	0.8073
$Fe_{0.0821}Co_3Al_1$	0.3086	2.3100	39	26	$Fe_{0.0821}Co_3Al_1O_x$	33	0.8076
$Fe_{0.1150}Co_3Al_1$	0.3085	2.3065	39	28	$Fe_{0.1150}Co_3Al_1O_x$	33	0.8093
$Fe_{0.1725}Co_3Al_1$	0.3081	2.2839	34	28	$Fe_{0.1725}Co_3Al_1O_x$	30	0.8083
$Fe_{0.2300}Co_3Al_1$	0.3081	2.2790	42	30	$Fe_{0.2300}Co_3Al_1O_x$	31	0.8096

Table 2 lists the specific surface areas (S_{BET}) of the (Mn,Fe)-Co-Al mixed metal oxides. S_{BET} for Co-Al-O_x of 82 m^2/g, significantly decreased after introduction of Mn or Fe within its structure. A similar trend was observed for both series, i.e. decrease for materials with 0.0821 mol.% then increase up to 0.1725 mol.%, and finally drop in S_{BET} for materials with the highest loading of transition metal (0.2300 mol.%). However, slightly higher values for S_{BET} were reached over Mn-containing mixed metal oxides. Chemical analysis identified by ICP-MS evidenced sodium residual from preparation procedure up to 2.3 wt.%.

Table 2. Total mass losses of (Mn,Fe)-Co-Al hydrotalcite-like compounds, specific surface areas (S_{BET}), sodium residuals of mixed metal oxides, and T_{50} of mixed metal oxides in N_2O/N_2, $N_2O,NO,O_2/N_2$* and $N_2O,H_2O/He$** gas mixtures.

Hydrotalcite-like compounds	Total mass loss [%]	Mixed metal oxides	S_{BET} [m^2/g]	Na [wt.%]	T_{50} [° C]
Co_3Al_1	32.62	$Co_3Al_1O_x$	82	1.4	352[a] *409[a] **549[b]
$Mn_{0.0575}Co_3Al_1$	31.90	$Mn_{0.0575}Co_3Al_1O_x$	59	0.7	317[a]
$Mn_{0.0821}Co_3Al_1$	31.54	$Mn_{0.0821}Co_3Al_1O_x$	57	1.3	332[a]
$Mn_{0.1150}Co_3Al_1$	30.53	$Mn_{0.1150}Co_3Al_1O_x$	61	1.0	320[a]
$Mn_{0.1725}Co_3Al_1$	30.89	$Mn_{0.1725}Co_3Al_1O_x$	76	2.3	305[a] *376[a] **528[b]
$Mn_{0.2300}Co_3Al_1$	31.03	$Mn_{0.2300}Co_3Al_1O_x$	65	0.8	316[a]
$Fe_{0.0575}Co_3Al_1$	31.43	$Fe_{0.0575}Co_3Al_1O_x$	56	0.8	356[a]
$Fe_{0.0821}Co_3Al_1$	31.34	$Fe_{0.0821}Co_3Al_1O_x$	53	0.8	325[a]
$Fe_{0.1150}Co_3Al_1$	31.10	$Fe_{0.1150}Co_3Al_1O_x$	54	1.6	333[a]
$Fe_{0.1725}Co_3Al_1$	30.27	$Fe_{0.1725}Co_3Al_1O_x$	54	0.9	327[a] *380[a] **549[b]
$Fe_{0.2300}Co_3Al_1$	31.00	$Fe_{0.2300}Co_3Al_1O_x$	50	0.9	355[a]

[a]350 mg of catalyst, 100 cm^3/min total flow; [b]70 mg of catalyst, 75 cm^3/min total flow.

Fig. 4 presents the H_2-TPR profiles for the Co_3Al_1 and selected $Mn(Fe)_xCo_3Al_1$ (x = 0.1725, 0.2300, mol.%) mixed metal oxides. The H_2-TPR profile for Co_3Al material revealed the presence of two main reduction peaks, with maxima centered at around 465 and 839 °C. The peak at lower temperatures appeared due to the complete reduction of Co_3O_4 to metallic cobalt [25–27]. While the high temperature reduction peak was related to the reduction of cobalt in $Co_2AlO_4/CoAl_2O_4$ [28]. $Mn(Fe)_xCo_3Al$ (x = 0.1725, 0.2300, mol.%) revealed similar H_2-TPR profiles to Co_3Al_1. However, the modification of Co_3Al with Mn or Fe

influenced its redox properties, i.e. the position of the first reduction peaks shifted to higher temperatures for Mn- or Fe-doped materials than for Co_3Al_1, while the position of the second peak shifted to lower temperatures, indicating depressed reducibility of Co_3O_4 and improved of cobalt in Co_2AlO_4 and $CoAl_2O_4$. Such effect was more visible for $FeCoAlO_x$. Additionally, for the Fe-containing samples a broad shoulder appeared at about 700 °C possibly due to reduction of iron oxide species [4,5]. Table 3 summarizes H_2-TPR data of the studied materials. The H_2 uptake varied in the range of 5.22-6.64 mmol/g in the temperature range of 50-530 °C (where N_2O decomposition proceeded). Furthermore, analysis of reduction peak areas (A^b/A^c, estimated from the integrated areas of the respective H_2-TPR peaks) revealed comparable ratio (0.29 to 0.35) across the samples. Due to different oxidation states of metal oxide species in spinel forms, the calculations of the H_2 uptake based on materials composition could be speculative. Fig. 5 shows the Co 2p, O 1s, Mn 2p and Fe 2p XPS spectra of $Co_3Al_1O_x$ and $Mn(Fe)_{0.1725}Co_3Al_1O_x$, while Table 3 summarizes the peaks positions, their binding energies, peak areas, full with at half maximum (FWHM) and $O_\alpha/(O_\beta+O_\gamma)$ molar ratio. The Co 2p XPS spectra exhibited two main peaks characterized by binding energies in the ranges of 781.6-779.6 and 796.9-795.0 eV corresponding to the $Co2p_{3/2}$ and $2p_{1/2}$ spin-orbit peaks, respectively [29]. Thus, since the spin-orbit values for the tested materials have varied in the range of 15.3-15.4 eV, we concluded that mainly Co_3O_4 (spin-orbit value of 15.2 eV) together with $CoAl_2O_4$ (as minor compound; spin-orbit value of 15.9 eV) existed on the catalysts surface [29–31]. Considering that Mn or Fe are present only in small amounts in the materials, determination of manganese or iron chemical state in the measured $Mn(Fe)_{0.1725}Co_3Al_1O_x$ based on the position of the binding energy could be speculative. Furthermore, Mn or Fe may be present in several chemical states with the overlapping spectra, which are close in energy [11,32]. The O 1s spectra were deconvoluted to lattice oxygen – O_α, surface adsorbed oxygen, OH groups and oxygen vacancies – O_β and adsorbed molecular water – O_γ [33]. Additional low peaks at about 527-528 eV appeared possibly due to the differential charging of the materials [34]. The molar ratio of $O_\alpha/(O_\beta+O_\gamma)$ varied in the range of 0.21-0.32.

Fig. 4, Fig. 5

Table 3. Amounts of H_2 consumed during H_2-TPR measurements (H_2 uptake), the peaks positions, their binding energies, peak areas, full with at half maximum (FWHM) and $O_\alpha/(O_\beta+O_\gamma)$ molar ratio of mixed metal oxides.

Mixed metal oxides	H_2 uptake[a] [mmol/g]	A[b]/A[c] [a.u.]	Position Co $2p_{3/2}$ *O 1s ■Mn $2p_{3/2}$ □Fe $2p_{3/2}$	FWHM [eV]	Area [a.u.]	$O_\alpha/(O_\beta+O_\gamma)$[d]
$Co_3Al_1O_x$	26.48	0.33	780.35	4.09	11998	
	6.64[b]		786.26	7.90	4073	
	19.84[c]		802.84	6.75	2239	
			*527.07	1.72	462	
			*528.77	1.92	2066	0.23
			*530.38	2.08	6369	
			*531.91	2.10	2697	
$Mn_{0.1725}Co_3Al_1O_x$	22.84	0.35	781.63	3.79	8333	
	5.90[b]		785.80	8.90	2826	
	16.94[c]		804.53	8.64	1134	
			*528.51	1.43	239	
			*530.07	2.09	2126	0.21
			*531.72	2.25	7926	
			*533.41	1.95	2106	
			■643.03	4.00	1080	
$Fe_{0.1725}Co_3Al_1O_x$	23.46	0.29	779.63	3.94	7137	
	5.22[b]		784.18	8.19	2085	
	18.24[c]		802.17	8.64	1244	
			*526.58	1.63	324	
			*528.37	2.20	2077	0.32
			*529.81	2.04	4523	
			*531.28	2.06	1933	
			□710.44	5.20	956	

[a]Calculated by equation: Y = 1E-08X + 1E-07, R^2 = 0.9996, and X, Y referred to the area of each reduction peak and the H_2 consumption, respectively. [b]In the region 50-530 °C. [c]In the region 530-1000 °C. [d]Estimated from the integrated areas of the respective XPS peaks.

Fig. 6 shows the XANES spectra of $Mn(Fe)_{0.1725}Co_3Al_1O_x$ mixed metal oxides. In comparison to the Co_3O_4 reference spectrum (Co K-edge), the spectrum of $Mn_{0.1725}Co_3Al_1O_x$ at room temperature showed a more intense pre-edge peak which could be rationalized as being caused by a greater degree of Co in a non-centrosymmetric geometry in this sample. Furthermore, an adsorption edge at lower energies – 7717.100 eV at room temperature versus 7716.440 eV after the thermal treatment in He – indicated a lower overall Co oxidation state (Fig 6A). This suggested the presence of a $CoAl_2O_4$ type spinel where the substitution of Co^{3+} by Al^{3+} in the octahedral position leads to a higher contribution of Co^{2+} Td. Indeed it has previously been shown that $CoAl_2O_4$ type

spinel phase can form at temperatures as low as 390 °C [35]. The Mn K-edge spectra acquired at room temperature (Fig. 6B) closely resembled that of a Mn_3O_4 spinel reported previously [36]. To date no XAFS data exists concerning mixed Mn and Co spinels although a detailed XRD/vibrational spectroscopic study of Co/Mn substitution suggests that such phases can readily be formed and therefore a mixed $Mn_xCo_yO_4$ and/or $Mn_xCo_yAl_zO_4$ could be present in our $Mn_{0.1725}Co_3Al_1O_x$ [37]. For $Fe_{0.1725}Co_3Al_1O_x$ mixed metal oxides measured at room temperature, Co K-edge XANES revealed comparable Co speciation to the Mn-containing sample (Fig. 6E). Nevertheless, the Fe near-edge spectrum closely resembled that of α-Fe_2O_3 (Fig. 6F), suggesting that unlike Mn, Fe did not incorporate so readily into the Co_3O_4 structure. In agreement, our H_2-TPR results showed separate reduction of iron oxide species in $Fe_{0.1725}Co_3Al_1O_x$; however, the shift to higher temperatures of Co_3O_4 reduction peak suggests that small amounts of iron must have incorporated into the spinel structure thereby affecting its redox properties.

Changes occurring in $Mn_{0.1725}Co_3Al_1O_x$ mixed metal oxides, in the presence of He and N_2O/He, were followed by studying the Co and Mn K-edge XANES spectra between room temperature and 600 °C. A shift in the Co absorption edge to lower energies as well as a decrease in the pre-edge intensity were observed upon He treatment at 600 °C, which is also consistent with a decrease in the nominal valence of Co in the material (Fig. 6A). The spectra resembled that of the CoO reference constituted by Co^{2+} in an octahedral environment. However, the sample's higher pre-edge intensity when compared to CoO/Co_3O_4 suggested some Co^{2+} was still present in a tetrahedral environment. Considering the H_2-TPR results pertaining to the reducibility of both cobalt oxide species present in the catalyst, it seems that $Mn_xCo_yO_4$ is reduced to (Mn)CoO while $CoAl_2O_4$, with Co^{2+} in a tetrahedral environment, remained unchanged. EXAFS *k*-plots for Co and Mn in $Mn_{0.1725}Co_3Al_1O_x$ before and after reduction are shown in Fig.1S. in the supplementary information. At room temperature the Mn and Co fine structure resembled closely the Co_3O_4 reference while in the reduced sample the fine structure is similar to CoO. This further confirms the presence of the initial spinel environment for both Mn and Co and that in both cases this evolves into the rock salt $M^{2+}O$ phase. Similar to Co, Mn also undergoes reduction upon activation in He at 600 °C; the reduced spectra resembling features of MnO [36]. Finally, in the presence of N_2O/He, both Co and Mn oxide species reoxidized to their initial state. Fig 6C and D show the temperature dependence of this reoxidation process; the spectral changes were observed at 300-450 °C

temperature range which coincided with the temperature needed to obtain full N_2O conversion. The MnO appeared easier to reoxidize than CoO since the spectral changes in Mn K-edge XANES commenced at 300 °C while changes in Co K-edge occurred at 350 °C.

Furthermore, the changes in the oxidation state of Co at different reaction stages in $Mn_{0.1725}Co_3Al_1O_x$ were studied by the investigation of the position of the absorption edge (defined as the first maximum of the derivative plot beyond the pre-edge peak). Table 4 presents the Co K-edge absorption positions relative to Co foil ($\Delta E = E_{sample} - E_{foil}$) of $Mn_{0.1725}Co_3Al_1O_x$ mixed metal oxides at different stages of the experiment as well as the ΔE of Co_3O_4 and CoO as references. Again, the ΔE of the sample after treatment with He at 600 °C was comparable to CoO. While the reoxidation, under N_2O/He conditions, leads to the recovery of its initial oxidation state. Table 5 lists the results of the curve-fitting analysis for the first coordination shell. First shell quick fit analysis of the EXAFS was carried out to gain insight into the average Co-O distances and coordination numbers. Fitting revealed higher coordination numbers and Co-O bond distances of 0.208 nm for $Mn_{0.1725}Co_3Al_1O_x$ mixed metal oxide pretreated with He at 600 °C, which is consistent with the appearance of CoO type structure. Otherwise, $Mn_{0.1725}Co_3Al_1O_x$ at room temperature or in the presence of N_2O/He at 600 °C showed a shorter Co-O of ~0.191 nm, corresponding to the presence of a majority spinel phase. As expected from XANES, the Co-O shell fitting results $Mn_{0.1725}Co_3Al_1O_x$ and $Fe_{0.1725}Co_3Al_1O_x$ at room temperature gave very similar results.

Fig. 6

Table 4. Co K-edge energy positions relative to Co foil (E_0) for $Mn_{0.1725}Co_3Al_1O_x$ mixed metal oxides at room temperature, after reduction under He and after reoxidation under N_2O/He at 600 °C as well as references at room temperature.

Mixed metal oxides	ΔE [eV]	References	ΔE [eV]
$Mn_{0.1725}Co_3Al_1O_x$		room temperature	
room temperature	8.1	CoO	7.4
600 °C He	7.4	Co_3O_4	8.5
600 °C N_2O/He	8.1		

Table 5. Coordination numbers (CN), bond distances between adsorbed and backscatter atoms (R), inner potential corrections to account for the difference in the inner potential between the sample and the reference compound (E), Debye-Waller factors ($2\sigma^2$), and residual factors (Rf) of $Mn_{0.1725}Co_3Al_1O_x$ mixed metal oxides.

Mixed metal oxides	Shell Co-O	CN	R [nm]	ΔE_0 [eV]	$10^2*\sigma^2$ [nm]	R_f [%]
$Fe_{0.1725}Co_3Al_1O_x$						
room temperature He		2.9	0.192	4.65	0.012	0.16
$Mn_{0.1725}Co_3Al_1O_x$						
room temperature He		2.8	0.191	4.64	0.016	1.30
after He 600 °C		4	0.208	2.29	0.16	3.2
after N_2O 600 °C		2.2	0.191	5.40	0.084	1.9

Fig. 7 presents the results of catalytic tests performed over $Mn(Fe)_xCo_3Al_1$ (x = 0.0575, 0.0821, 0.1150, 0.1725, 0.2300, mol.%) mixed metal oxides, while Table 2 lists temperature necessary to obtain 50% N_2O conversion (T_{50}). The N_2O conversion from the reaction mixture started at about 150-200 °C, while full conversion was reached at about 450-500 °C for all tested materials. Co_3Al_1 reached T_{50} at about 352 °C with the full conversion at 500 °C. Incorporation of Mn or Fe into Co_3Al_1 structure improved catalytic activity of mixed metal oxides. An exception was $Fe_{0.2300}Co_3Al_1$, which showed catalytic activity similar to Co_3Al_1. Reproducibility of our results of catalytic tests was confirmed by repeated measurements. The activity differentiated among tested materials without clear trend neither related to the Mn or Fe nor Na (up to 2.3 wt.%) content in the materials. Obalová et al. [32] pointed out that 1.15 wt.% of Na introduced by impregnation already slightly enhanced activity of Co_4MnAlO_x. While materials with Na loaded by impregnation was reported to facilitate N_2O decomposition than materials with Na present after preparation procedure [33,34]. The optimum of deposited Na content varied also depending on the applied mixed metal oxides: 0.75 wt.% for $Co_{2.5}Rh_{0.05}Al_1O_x$ [33], 1.5 wt.% for $Co_3Al_1O_x$ [35] or 1.4 wt.% for $Co_4Mn_1Al_1O_x$ [36]. Farris et al. [37] found out an optimum Na residual content in the range of 3.0-6.0 wt.% in Co-Al-O_x was supposed to promote the decomposition of N_2O facilitating over 80% conversion at 475 °C. Doping with 1.0-2.0 wt.% of Na resulted in comparable results. Further research should be carried out in order to clarify these remarkable observations over investigated mixed metal oxides.

The highest activity among tested materials reached $Mn_{0.1725}Co_3Al_1$. ~~Such catalyst reached~~ with T_{50} at 305 °C ~~with~~ and full conversion at 400 °C. Furthermore, $Mn_{0.1725}Co_3Al_1$ possessed similar activity to the Ag-doped catalysts – (0.7 wt.%)$AgCo_3(Mg_1)Al_1$, and only slightly lower to the (0.7 wt.%)$RhCo_3Mg_1Al_1$, reported as one of the most active and stable hydrotalcite derived mixed metal oxides in the N_2O decomposition with excellent activity and stability performance [7,38]. Catalytic tests were carried out under the same reaction conditions (Fig. 6C). Co_3Al_1 and $Mn(Fe)_{0.1725}Co_3Al_1$ were also tested in the presence of NO and O_2 (350 mg of catalyst, 100 cm^3/min total flow). $Mn_{0.1725}Co_3Al_1$ presented T_{50} of 376 °C, thus temperature of about 70 °C higher than for tests without NO and O_2. Slightly lower activity above 350 °C was obtained over $Fe_{0.1725}Co_3Al_1$ with T_{50} at 380 °C. Furthermore, for practical applications, Co_3Al_1 and $Mn(Fe)_{0.1725}Co_3Al_1$ were tested in the presence of H_2O (70 mg of catalyst, 75 cm^3/min), as displayed on Fig. 2SA. The highest resistance to water vapour showed $Mn_{0.1725}Co_3Al_1$ with T_{50} of 549 °C. Other materials presented significantly lower resistance to water vapour. Fig. 2SB presents the contribution of NO formation over Co_3Al_1 and $Mn(Fe)_{0.1725}Co_3Al_1$. The highest amount of such by-product in N_2O decomposition appeared over $Fe_{0.1725}Co_3Al_1$. For other materials the formation of NO did not exceed 15 ppm in the studied temperatures of 200-550 °C. Notably, for catalytic tests carried out in the presence of water vapour NO formation decreased. In Fig. 3S, a time-on-stream tests was conducted to evaluate the stability of Co_3Al_1 and $Mn(Fe)_{0.1725}Co_3Al_1$ at 450 °C. All materials showed stable conversion during first 85 min in the N_2O/N_2 feed. Subsequently, after introduction water vapour into the feed, the conversion for all materials significantly dropped, and reached stable level below 20%. However, switching from wet to dry reaction mixture resulted in an increase of the catalysts conversion to the former level. Thus, the introduction of H_2O into the feed did not result in the permanent deactivation of the catalysts.

Obalová et al. [10,16] reported that the high activity of $Co_4Mn_1Al_1$ hydrotalcite derived mixed metal oxides appeared due to an optimum content of components reducible in the temperatures of the maximum conversion of N_2O (between 350-450 °C). Analysis of our reduction peak areas showed similar ratio (0.29 to 0.35) across the samples. Crystal sizes were calculated from (3 1 1) brag reflection in the XRD patterns using the Scherrer equation; the comparable results of 27, 26 and 30 nm for $Co_3Al_1O_x$, $Mn_{0.1725}Co_3Al_1O_x$ and $Fe_{0.1725}Co_3Al_1O_x$ respectively discard size effects in the catalytic performance. Although, the strength of lattice oxygen-metal bonds was reported to determine the catalysts activity in deN_2O [11], we did not observe clear correlation

between $O_\alpha/(O_\beta+O_\gamma)$ molar ratio and catalytic activity of mixed metal oxides. ~~Thus it seems that the samples' different reactivity was related mainly to the Mn and Fe speciation observed by XAS.~~ Mn in $Mn_{0.1725}Co_3Al_1O_x$ appeared incorporated within spinel structure; MnO and CoO phases present after activation reoxidize under N_2O/He feed. ~~showing that both take part in redox processes for deN_2O. Indeed it appears that MnO seemed to undergo faster reoxidation suggesting it may act as better electron donor in N_2O activation step considered the rate-determining stem of the mechanism [39,40].~~ Indeed this observation of Mn being easier to oxidise back to 3+ than Co, yet harder to reduce to 2+ is completely consistent with the respective redox potentials for the two elements [31]. Iron in $Fe_{0.1725}Co_3Al_1O_x$ could have similar role as Mn due to its higher oxidability compared with cobalt oxides. Nevertheless, as most of the iron was not incorporated to the spinel but appeared as separate Fe_2O_3 phase, its effect in catalytic activity was less pronounced than for Mn in the $Mn_{0.1725}Co_3Al_1O_x$ sample. Accordingly, decomposition of N_2O over tested mixed metal oxides followed the cationic redox mechanism [11,24], consisting of N_2O activation by electron transfer from metal sites, and diffusive recombination of the surface oxygen intermediates into oxygen, concerted with the back electron transfer that restores the oxidation state of the active sites. The regeneration of the active sites through oxygen desorption is considered as the rate-determining step. In this context, Co oxidizes when N_2O is adsorbed and then Co is again reduced when O_2 is released. Thus, during reaction under N_2O/He conditions, Co is continuously oxidizing and reducing. The doping, in particular Mn, may generate new redox sites at the surface or may enhance the oxygen desorption from cobalt sites. Taking into account the very weak amount of manganese added and the fact that manganese appeared incorporated within structure, the latter assumption seems more likely.

Fig. 7

4. Conclusion

$Mn(Fe)_xCo_3Al_1$ (x = 0.0575, 0.0821, 0.115, 0.1725 and 0.2300, mol.%) hydrotalcite derived mixed metal oxides were synthesized by coprecipitation and subsequent calcination. The catalytic activity of Co_3Al_1 mixed metal oxides was improved in deN_2O by incorporation of appropriate amount of Mn or Fe. $Mn_{0.1725}Co_3A_l$ mixed metal

oxides reached the highest activity with T_{50} of about 305 and 376 °C under N_2O/N_2 and $N_2O,NO,O_2/N_2$ feed, respectively. The trend for catalytic conversion was $Mn_{0.1725}Co_3Al_lO_x$ > $Fe_{0.1725}Co_3Al_lO_x$ > $Co_3Al_lO_x$. Detailed evaluation of the active species was realized by *in situ* XAFS study. Correlation of the catalytic data with the XAS results suggested that doping Co_yO_4 spinel by Mn (Fe), easier to oxidise, leads to a better facility to desorb oxygen ~~, as the active phase for deN_2O~~. The presence of Mn in the spinel structure seemed to provide surface Co active sites easier to release oxygen. The lower activity of the $Fe_{0.1725}Co_3Al_lO_4$ mixed metal oxides was attributed to the fact that Fe did not incorporate so readily into the cobalt spinel structure forming less active iron oxide clusters instead.

Acknowledgements

Funded by the Excellence Initiative of the German federal and state governments in the frame of the Center for Automotive Catalytic Systems Aachen (ACA) at RWTH Aachen University. The authors acknowledge the Diamond Light Source (project SP14834) for provision of beamtime on the beamlines B18, and Diego Gianolio for assistance in performing the XAFS measurements. The authors thank Andreas Holz for the assistance in preparation, characterization and catalytic tests.

References

[1] M. Jablonska, R. Palkovits, Nitrogen oxide removal over hydrotalcite-derived mixed metal oxides, Catal. Sci. Technol. 6 (2016) 49–72.

[2] F. Cavani, F. Trifirò, A. Vaccari, Hydrotalcite-type anionic clays: Preparation, properties and applications., Catal. Today. 11 (1991) 173–301.

[3] A. Vaccari, Preparation and catalytic properties of cationic and anionic clays, Catal. Today. 41 (1998) 53–71.

[4] L. Chmielarz, A. W\kegrzyn, M. Wojciechowska, S. Witkowski, M. Michalik, Selective Catalytic Oxidation (SCO) of Ammonia to Nitrogen over Hydrotalcite Originated Mg--Cu--Fe Mixed Metal Oxides, Catal. Letters. 141 (2011) 1345–1354.

[5] M. Jabłońska, L. Chmielarz, A. W\kegrzyn, K. Guzik, Z. Piwowarska, S. Witkowski, R.I. Walton, P.W.

Dunne, F. Kovanda, Thermal transformations of Cu--Mg (Zn)--Al(Fe) hydrotalcite-like materials into metal oxide systems and their catalytic activity in selective oxidation of ammonia to dinitrogen, J. Therm. Anal. Calorim. 114 (2013) 731–747.

[6] M. Jabłońska, K. Nothdurft, M. Nocuń, V. Girman, R. Palkovits, Redox-performance correlations in Ag–Cu–Mg–Al, Ce–Cu–Mg–Al, and Ga–Cu–Mg–Al hydrotalcite derived mixed metal oxides, Appl. Catal. B Environ. 207 (2017) 385–396.

[7] M. Jablonska, R. Palkovits, It is no laughing matter: nitrous oxide formation in diesel engines and advances in its abatement over rhodium-based catalysts, Catal. Sci. Technol. 6 (2016) 7671–7687.

[8] J. Pérez-Ramírez, J. Overeijnder, F. Kapteijn, J.A. Moulijn, Structural promotion and stabilizing effect of Mg in the catalytic decomposition of nitrous oxide over calcined hydrotalcite-like compounds, Appl. Catal. B Environ. 23 (1999) 59–72.

[9] J. Pérez-Ramírez, F. Kapteijn, J.A. Moulijn, High activity and stability of the Rh-free Co-based ex-hydrotalcite containing Pd in the catalytic decomposition of N2O, Catal. Letters. 60 (1999) 133–138.

[10] L. Obalová, K. Jirátová, F. Kovanda, K. Pacultová, Z. Lacný, Z. Mikulová, Catalytic decomposition of nitrous oxide over catalysts prepared from Co/Mg-Mn/Al hydrotalcite-like compounds, Appl. Catal. B Environ. 60 (2005) 289–297.

[11] L. Obalová, K. Pacultová, J. Balabánová, K. Jirátová, Z. Bastl, M. Valášková, Z. Lacný, F. Kovanda, Effect of Mn/Al ratio in Co–Mn–Al mixed oxide catalysts prepared from hydrotalcite-like precursors on catalytic decomposition of {N2O}, Catal. Today. 119 (2007) 233–238.

[12] L. Obalová, K. Karásková, A. Wach, P. Kustrowski, K. Mamulová-Kutláková, S. Michalik, K. Jirátová, Alkali metals as promoters in Co–Mn–Al mixed oxide for {N2O} decomposition, Appl. Catal. A Gen. 462–463 (2013) 227–235.

[13] L. Chmielarz, M. Rutkowska, P. Kuśtrowski, M. Drozdek, Z. Piwowarska, B. Dudek, R. Dziembaj, M. Michalik, An influence of thermal treatment conditions of hydrotalcite-like materials on their catalytic activity in the process of N2O decomposition, J. Therm. Anal. Calorim. 105 (2011) 161–170.

[14] J.N. Armor, T.A. Braymer, T.S. Farris, Y. Li, F.P. Petrocelli, E.L. Weist, S. Kannan, C.S. Swamy, Calcined hydrotalcites for the catalytic decomposition of N2O in simulated process streams, Appl. Catal.

B Environ. 7 (1996) 397–406.

[15] S. Kannan, Decomposition of nitrous oxide over the catalysts derived from hydrotalcite-like compounds, Appl. Clay Sci. 13 (1998) 347–362.

[16] S. Kannan, C.S. Swamy, Catalytic decomposition of nitrous oxide over calcined cobalt aluminum hydrotalcites, Catal. Today. 53 (1999) 725–737.

[17] F. Kovanda, T. Rojka, J. Dobešová, V. Machovič, P. Bezdička, L. Obalová, K. Jirátová, T. Grygar, Mixed oxides obtained from Co and Mn containing layered double hydroxides: Preparation, characterization, and catalytic properties, J. Solid State Chem. 179 (2006) 812–823.

[18] M. Newville, IFEFFIT: interactive XAFS analysis and FEFF fitting, J. Synchrotron Radiat. 8 (2001) 322–324.

[19] B. Ravel, M. Newville, ATHENA, ARTEMIS, HEPHAESTUS: data analysis for X-ray absorption spectroscopy using IFEFFIT, J. Synchrotron Radiat. 12 (2005) 537–541.

[20] S.P. Newman, W. Jones, P. O'Connor, D.N. Stamires, Synthesis of the 3R2 polytype of a hydrotalcite-like mineral, J. Mater. Chem. 12 (2002) 153–155.

[21] R.D. t Shannon, Revised effective ionic radii and systematic studies of interatomic distances in halides and chalcogenides, Acta Crystallogr. Sect. A Cryst. Physics, Diffraction, Theor. Gen. Crystallogr. 32 (1976) 751–767.

[22] A.L. Allred, E.G. Rochow, A scale of electronegativity based on electrostatic force, J. Inorg. Nucl. Chem. 5 (1958) 264–268.

[23] J. Perez-Ramirez, G. Mul, F. Kapteijn, J.A. Moulijn, A spectroscopic study of the effect of the trivalent cation on the thermal decomposition behaviour of Co-based hydrotalcites, J. Mater. Chem. 11 (2001) 2529–2536.

[24] A. Klyushina, K. Pacultová, K. Karásková, K. Jirátová, M. Ritz, D. Fridrichová, A. Volodarskaja, L. Obalová, Effect of preparation method on catalytic properties of Co-Mn-Al mixed oxides for N2O decomposition, J. Mol. Catal. A Chem. 425 (2016) 237–247.

[25] L. Chmielarz, Z. Piwowarska, M. Rutkowska, M. Wojciechowska, B. Dudek, S. Witkowski, M. Michalik, Total oxidation of selected mono-carbon {VOCs} over hydrotalcite originated metal oxide

catalysts, Catal. Commun. 17 (2012) 118–125.

[26] T. Franken, R. Palkovits, Investigation of potassium doped mixed spinels CuxCo3−xO4 as catalysts for an efficient {N2O} decomposition in real reaction conditions, Appl. Catal. B Environ. 176–177 (2015) 298–305.

[27] L. Xue, C. Zhang, H. He, Y. Teraoka, Catalytic decomposition of {N2O} over CeO2 promoted Co3O4 spinel catalyst, Appl. Catal. B Environ. 75 (2007) 167–174.

[28] E. Genty, J. Brunet, C. Poupin, S. Casale, S. Capelle, P. Massiani, S. Siffert, R. Cousin, Co-Al mixed oxides prepared via LDH route using microwaves or ultrasound: Application for catalytic toluene total oxidation, Catalysts. 5 (2015) 851–867.

[29] I.A.P.S. Murthy, C.S. Swamy, Catalytic decomposition of 2-propanol on Co1+xAl2−xO4 spinel system, Catal. Letters. 27 (1994) 103–112.

[30] J.-Y. Luo, M. Meng, X. Li, X.-G. Li, Y.-Q. Zha, T.-D. Hu, Y.-N. Xie, J. Zhang, Mesoporous Co3O4–CeO2 and Pd/Co3O4–CeO2 catalysts: Synthesis, characterization and mechanistic study of their catalytic properties for low-temperature CO oxidation, J. Catal. 254 (2008) 310–324.

[31] Z. Zhu, G. Lu, Z. Zhang, Y. Guo, Y. Guo, Y. Wang, Highly Active and Stable Co3O4/ZSM-5 Catalyst for Propane Oxidation: Effect of the Preparation Method, ACS Catal. 3 (2013) 1154–1164.

[32] P. Graat, M.A.J. Somers, Quantitative Analysis of Overlapping XPS Peaks by Spectrum Reconstruction: Determination of the Thickness and Composition of Thin Iron-oxide Films, Surf. Interface Anal. 26 (1998) 773–782.

[33] V.P. Santos, M.F.R. Pereira, J.J.M. Órfão, J.L. Figueiredo, The role of lattice oxygen on the activity of manganese oxides towards the oxidation of volatile organic compounds, Appl. Catal. B Environ. 99 (2010) 353–363.

[34] M. Konsolakis, Z. Ioakimidis, T. Kraia, G.E. Marnellos, Hydrogen Production by Ethanol Steam Reforming (ESR) over CeO2 Supported Transition Metal (Fe, Co, Ni, Cu) Catalysts: Insight into the Structure-Activity Relationship, Catalysts. 6 (2016).

[35] A.M. Beale, G. Sankar, Understanding the Crystallization of Nanosized Cobalt Aluminate Spinel from Ion-Exchanged Zeolites Using Combined in Situ QEXAFS/XRD, Chem. Mater. 18 (2006) 263–272.

[36] G. Zhang, F. Liu, H. Liu, J. Qu, R. Liu, Respective Role of Fe and Mn Oxide Contents for Arsenic Sorption in Iron and Manganese Binary Oxide: An X-ray Absorption Spectroscopy Investigation, Environ. Sci. Technol. 48 (2014) 10316–10322.

[37] P.L. Meena, R. Kumar, K. Sreenivas, Rietveld refinement and spectroscopic analysis of Co3-xMnxO4 ($0.1 \leq x \leq 1.0$) ceramic compositions, Int. J. Phys. Chem. Math. Sci. 3 (2014) 7.

[38] M. Konsolakis, Recent Advances on Nitrous Oxide (N2O) Decomposition over Non-Noble-Metal Oxide Catalysts: Catalytic Performance, Mechanistic Considerations, and Surface Chemistry Aspects, ACS Catal. 5 (2015) 6397–6421.

[39] K.S. Chang, H. Song, Y.-S. Park, J.-W. Woo, Analysis of N2O decomposition over fixed bed mixed metal oxide catalysts made from hydrotalcite-type precursors, Appl. Catal. A Gen. 273 (2004) 223–231.

[40] L. Obalová, V. Fíla, Kinetic analysis of N2O decomposition over calcined hydrotalcites, Appl. Catal. B Environ. 70 (2007) 353–359.

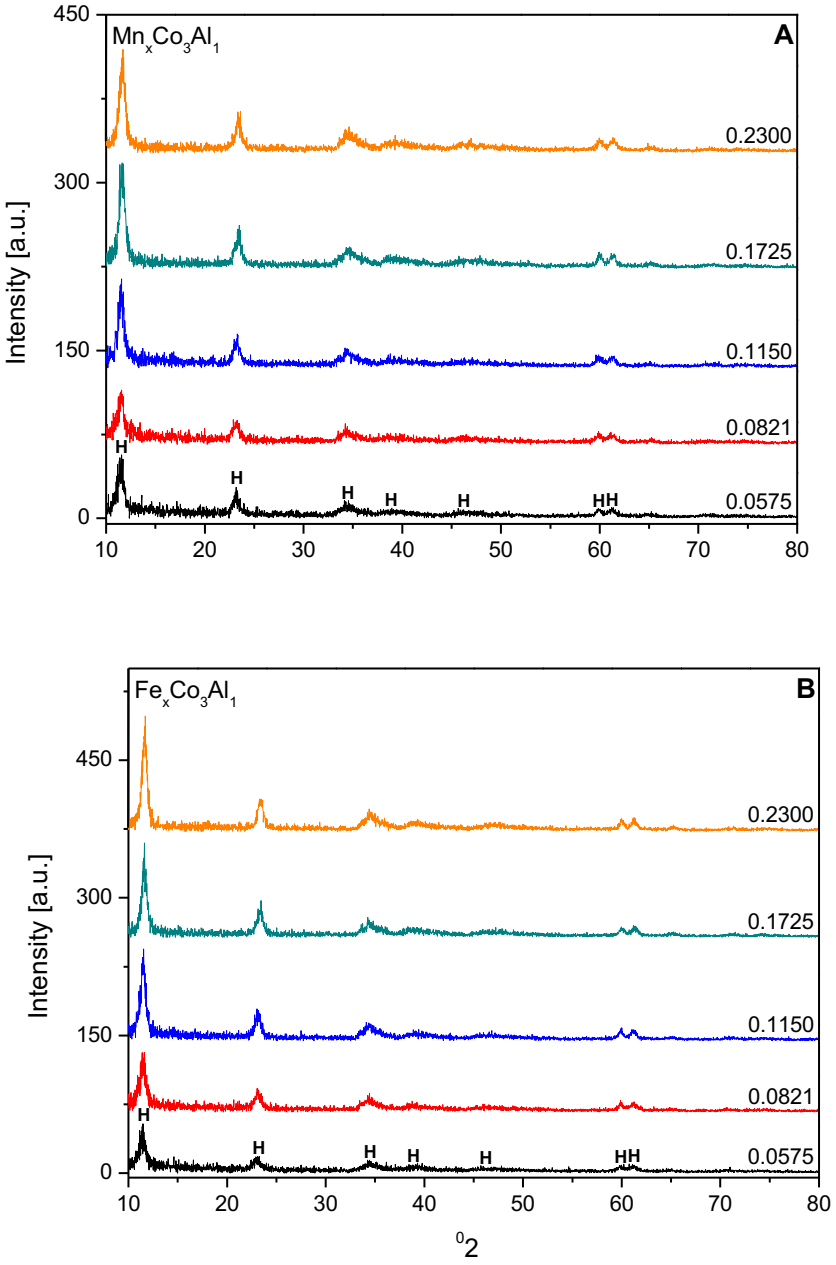

Fig. 1. X-ray diffraction patterns of Mn(Fe)-Co-Al hydrotalcite-like compounds; H – hydrotalcite-like phase.

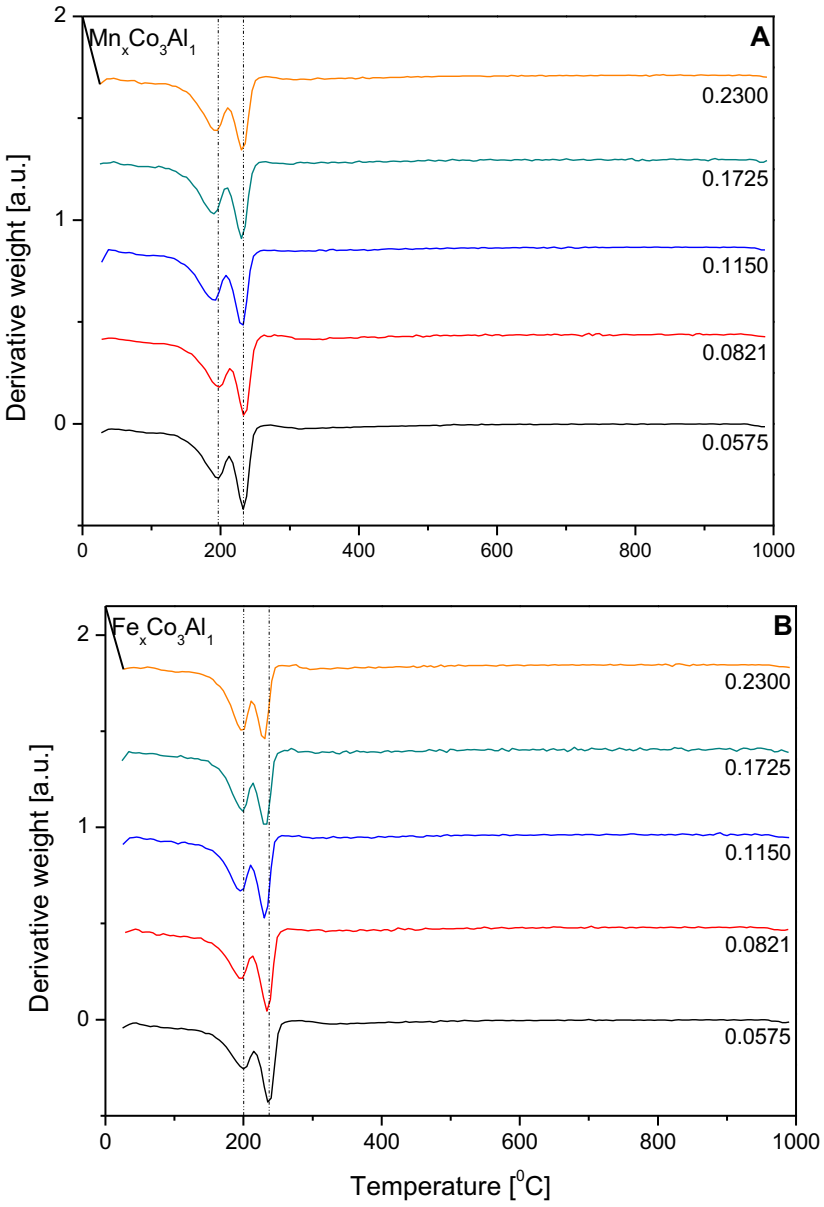

Fig. 2. DTG profiles of Mn(Fe)-Co-Al hydrotalcite-like compounds; experimental conditions: mass of sample = 20 mg, flow of synthetic air = 10 cm^3/min, liner heating rate of 5 K/min.

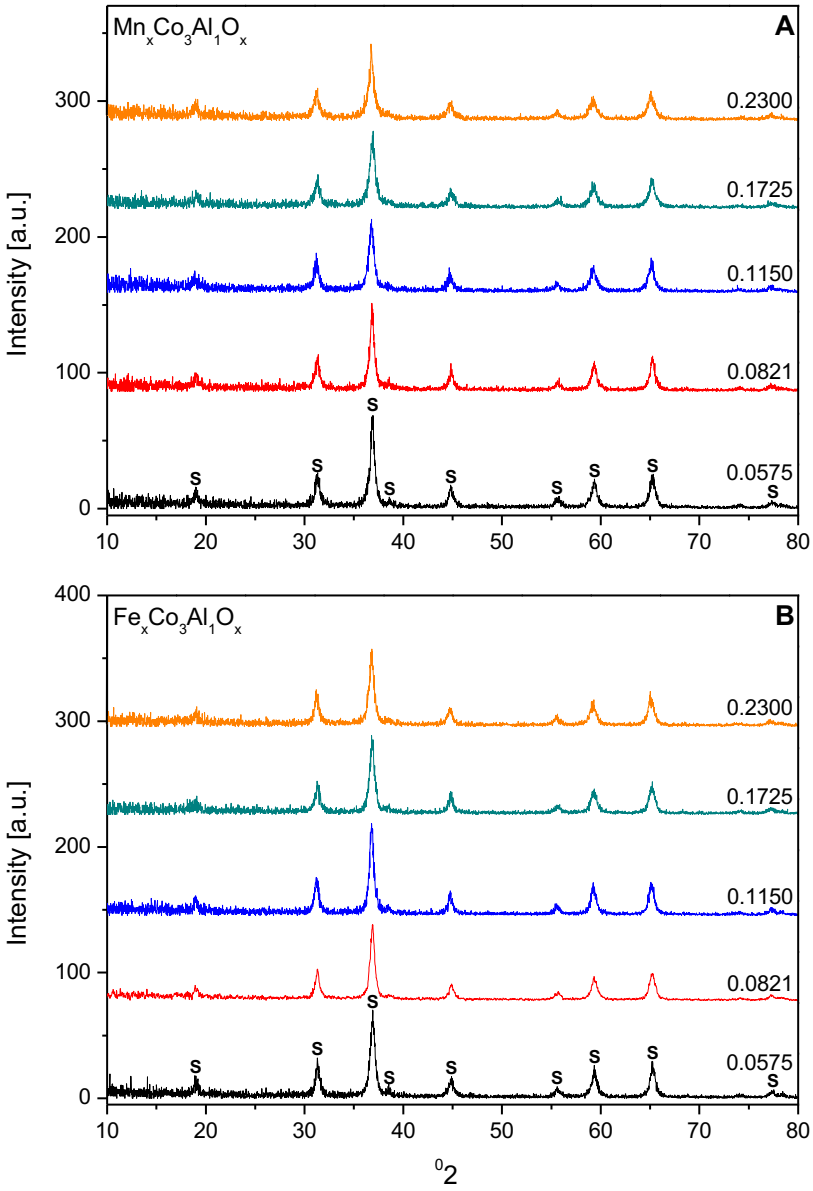

Fig. 3. X-ray diffraction patterns of Mn(Fe)-Co-Al mixed metal oxides; S – Co_3O_4/$CoAl_2O_4$/Co_2AlO_4.

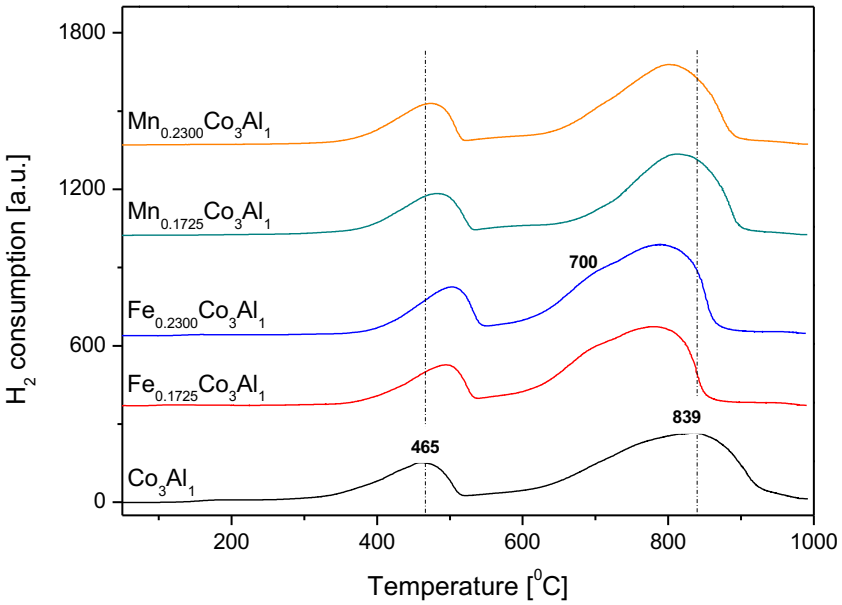

Fig. 4. H_2-TPR profiles of selected (Mn,Fe)-Co-Al mixed metal oxides; experimental conditions: mass of catalysts = 30 mg, [H_2] = 5.0 vol.%, [Ar] = 95.0 vol.%, flow rate = 25 cm^3/min, linear heating of 5 K/min.

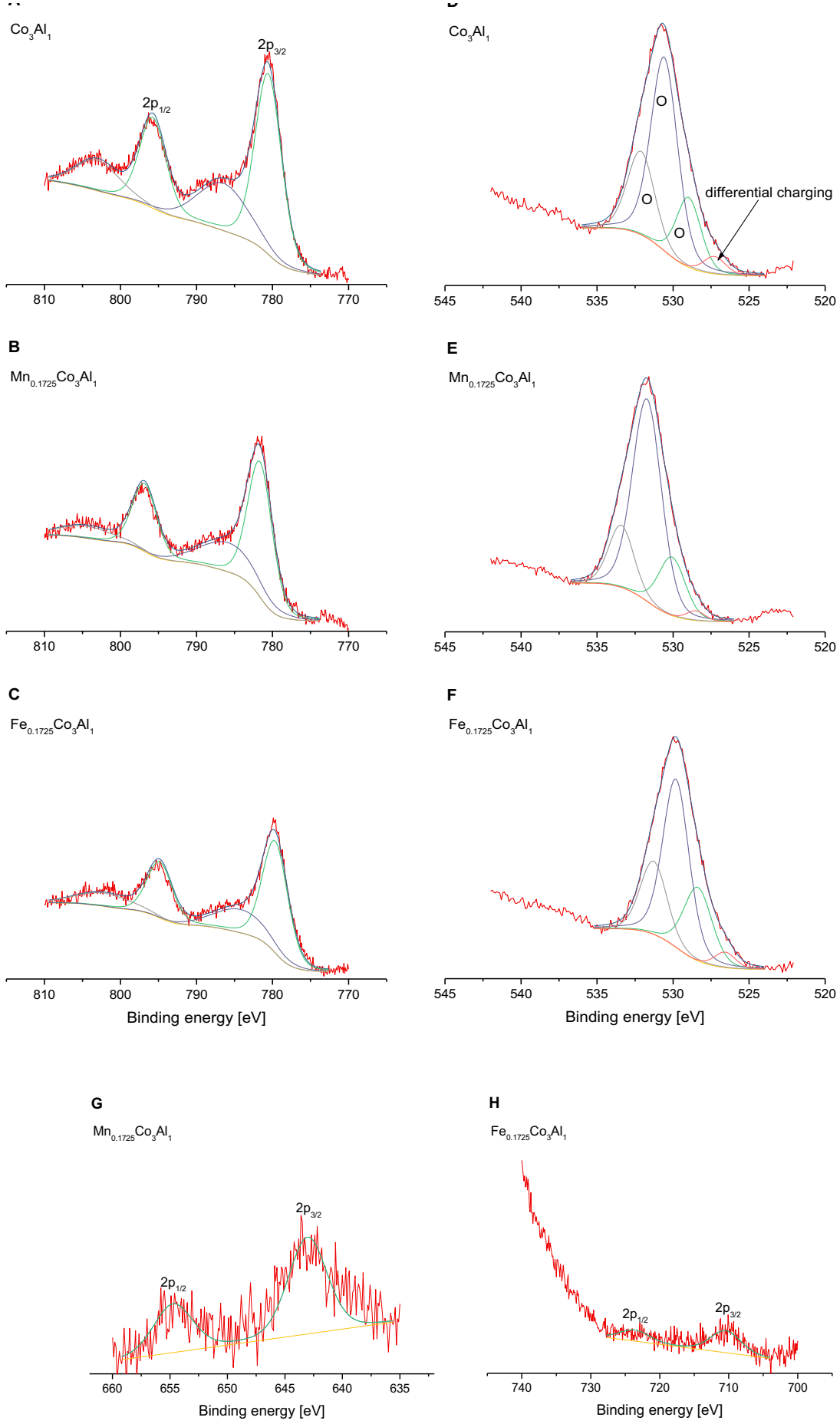

Fig. 5. XPS spectra of selected (Mn,Fe)-Co-Al mixed metal oxides; Co 2p (A-C), O 1s (D-F), Mn 2p (G) and Fe 2p (H).

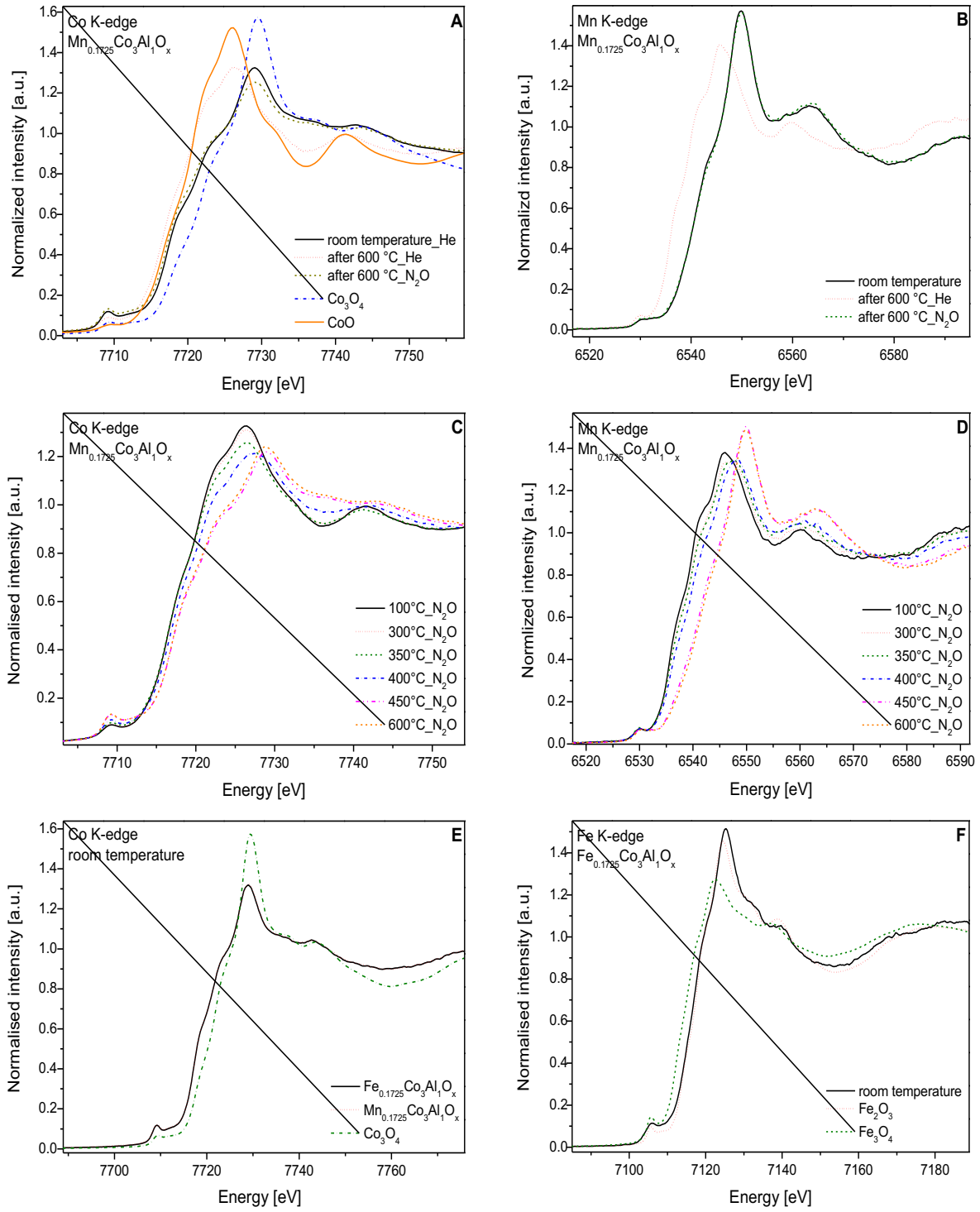

Fig. 6. *In situ* XANES spectra of A) Co K-edge for $Mn_{0.1725}Co_3Al_1O_x$ at different reaction stages and Co references; B) Mn K-edge for $Mn_{0.1725}Co_3Al_1O_x$ sample acquired at different stages of reaction; C) Co K-edge during the temperature ramp under N_2O; D) Mn K-edge during the temperature ram under N_2O; E) Co K-edge for $Mn_{0.1725}Co_3Al_1O_x$, $Fe_{0.1725}Co_3Al_1O_x$ and Co_3O_4 reference at room temperature; and F) Fe K-edge for $Fe_{0.1725}Co_3Al_1O_x$ and references.

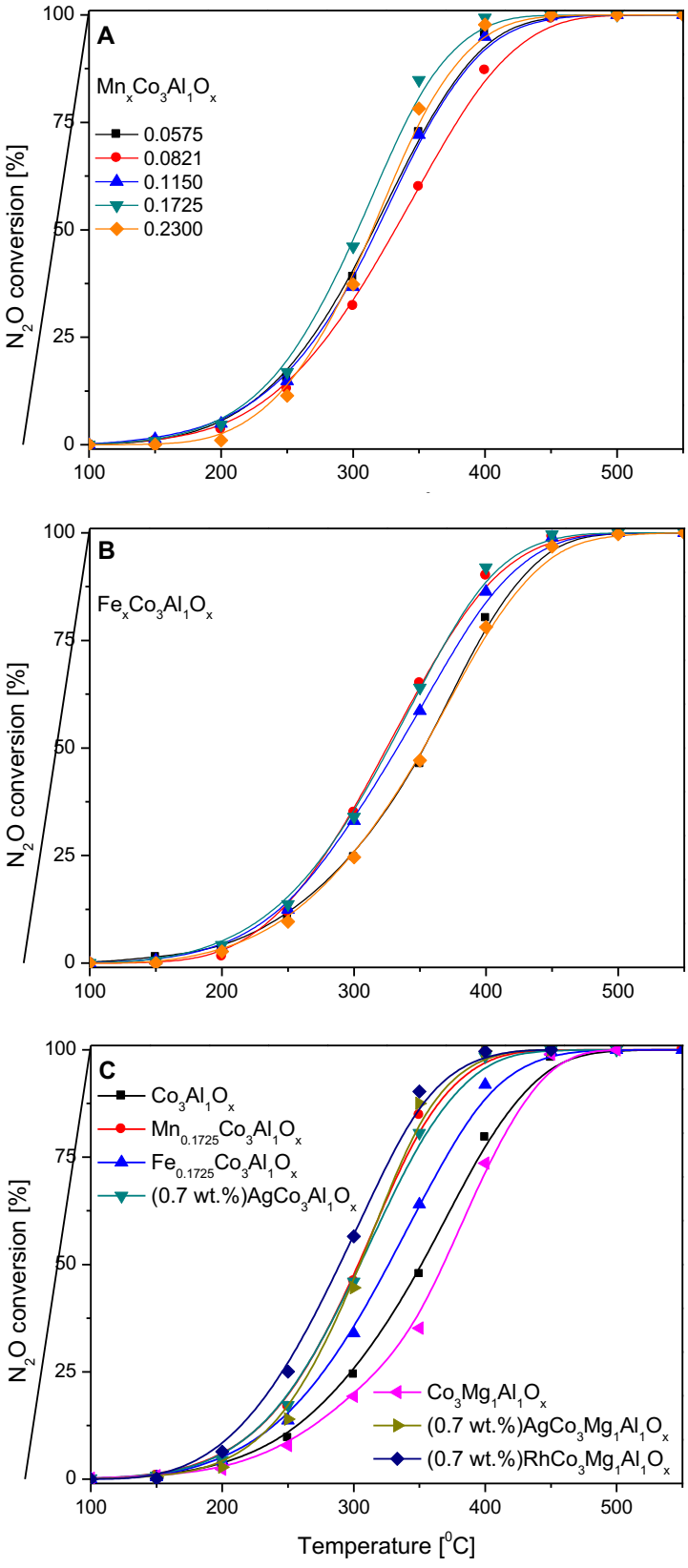

Fig. 7. Results of catalytic tests performed over Co_3Al_1, $(Mn,Fe)_xCo_3Al$ (x = 0, 0.0575, 0.0821, 0.1150, 0.1725, 0.2300) and (0.7 wt.%)Ag(Rh)$Co_3(Mg_1)Al_1$ mixed metal oxides; reaction conditions: mass of catalysts = 350 mg, $[N_2O]$ = 0.1 vol.%, N_2 balance, total flow rate = 100 cm^3/min, WHSV of 17 L $(h\ g)^{-1}$.